Advances in Nano Research, *Vol. 10, No. 5 (2021) 449-460*
DOI: https://doi.org/10.12989/anr.2021.10.5.449

Size-dependent flexoelectricity-based vibration characteristics of honeycomb sandwich plates with various boundary conditions

Zeinab Soleimani-Javid[1], Ehsan Arshid[1], Mohammad Khorasani[2], Saeed Amir[1] and Abdelouahed Tounsi*[3,4]

[1]*Department of Solid Mechanics, Faculty of Mechanical Engineering, University of Kashan, Kashan, Iran*
[2]*Department of Basic and Applied Sciences for Engineering, Sapienza University, Rome, Italy*
[3]*Yonsei Frontier Laboratory, Yonsei University, Seoul, Korea*
[4]*Department of Civil and Environmental Engineering, King Fahd University of Petroleum & Minerals, 31261 Dhahran, Eastern Province, Saudi Arabia*

(*Received April 22, 2020, Revised January 12, 2021, Accepted January 14, 2021*)

Abstract. Flexoelectricity is an interesting materials' property that is more touchable in small scales. This property beside the sandwich structures placed in the center of scientists' attention due to their extraordinary effects on the mechanical properties. Furthermore, in the passage of decades, more elaborated sandwich structures took into consideration results from using honeycomb core. This kind of structure, inspiring from honeycomb core, provides more stiffness to weight ratio, which plays a crucial role in different industries. In this paper, based on the Love-Kirchhoff's hypothesis, Hamilton's principle, modified couple stress theory and Fourier series analytical method, equations of motion for a sandwich plate containing a honeycomb core integrated by two face-sheets have derived and solved analytically. The equations of both face sheets have derived by flexoelectricity consideration. Moreover, it should be noticed that the whole structure rests on the visco-Pasternak foundation. Conducting current research provided an acceptable and throughout study based on flexoelectricity to address the effect of materials' characteristics, length-scale parameter, aspect, and thickness ratios and boundary conditions on the natural frequency of honeycomb sandwich plates. Also, based on the presented figures and tables, there is a close agreement between previous studies and recent work. Due to the high ratio of strength to weight, current model analyzing is capable of taking into account for different vehicles' manufacturing in a high range of industries.

Keywords: flexoelectricity; vibration analysis; sandwich plates; honeycomb core; modified couple stress theory

1. Introduction

Since many years ago, scientists examined various behaviors of a wide range of different mechanical structures in order to provide clearer mindset background for who are involved with such structures (Mehar *et al*. 2018, 2020a, b Singh *et al*. 2019, Bisen *et al*. 2020, Katariya and Panda 2019a). In this way, they considered different parameters to gain more accurate results (Katariya and Panda 2019b, Katariya *et al*. 2018, Hirwani and Panda 2018, 2019a, b). To have a complete understanding of what is analyzed in recent paper, it seems to be better to initiate this part with basic definitions. Piezoelectricity serves the linear response of polarization to mechanical strain and vice versa. On the other hand, flexoelectricity is a coupling between polarization and strain gradient, rather than between polarization and homogeneous strain. As another expression, piezoelectricity represents the linear coupling between electrical and mechanical variables, while flexoelectricity denotes the linear coupling between strain gradient and polarization (Yudin and Tagantsev 2013) and strain and polarization gradient (Mindlin 1968). It is also worthwhile mentioning that analogous to definitions of the direct and the converse piezoelectric effects, induction of the electric polarization due to the strain gradient has called direct flexoelectric effect and increasing mechanical stress or strain due to the electric field gradient has termed converse flexoelectric effect. Based on statistics, it has revealed that the flexoelectric effect is more significant in micro and nano-scale. Furthermore, honeycomb sandwich plates include a hexagonal honeycomb core and two homogenous face sheets.

One of the first works in honeycomb field backs to 1994, where Maheri and Adams had a study on steady-state flexural vibration damping of honeycomb sandwich beams (Maheri and Adams 1994). Then and in 2004, shock-absorbing characteristics and vibration transmissibility of honeycomb paperboard conducted by Guo and Jinghui. In this work, from the vibration tests with a slow sine sweep, the peak frequencies and vibration transmissibility are measured and used to estimate the damping ratios (Guo and Jinghui 2004). After that, in 2008, the free flexural vibration of symmetric rectangular honeycomb panels having SCSC edge supports has investigated using the classical plate theory and Reddy's third-order plate theory by Li and Jin

*Corresponding author, Professor,
E-mail: abdelouahed.tounsi@yonsei.ac.kr;
tou_abdel@yahoo.com

ISSN: 2287-237X (Print), 2287-2388 (Online)

(2008). In 2010, a semi-analytical method proposed for mechanical behavior analysis of sandwich panels with square honeycomb cores (Liu *et al*. 2010). Later and in 2016, an analytical framework was proposed by Mukhopadhyay and Adhikari to analyze the effect of random structural irregularity in honeycomb core for natural frequencies of sandwich panels. Their results suggest that spatially random irregularities in the honeycomb core have a considerable effect on the natural frequencies of sandwich panels (Mukhopadhyay and Adhikari 2016). Besides this, Kumar and Renji had a profound study on composite honeycomb sandwich panels subjected to diffuse acoustic field in a reverberation chamber in 2019, and they succeed in measuring strains (Kumar and Renji 2019). Earlier in 2020, Sobhy used differential quadrature method for magneto-hygrothermal bending investigation of functionally graded graphene/Al sandwich-curved beams with honeycomb core via a new higher-order theory (Sobhy 2020). Theoretical work on flexoelectricity dates back to 1957, where Mashkevich (1957) proposed the effect of flexoelectricity for the first time (Mashkevich 1957). After that, Kogan formulated this phenomenon. Kogan estimated the flexoelectric coefficients for crystal dielectrics with the order of $e/a = 10^{-9}$ *C/m*, where *e* is the electron charge, and a is the lattice parameter (Sharma *et al*. 2007). Tagantsev (1986) theoretically confirmed that the flexoelectric effect in the crystalline solids is different from the piezoelectric effect, and he derived a simple model for computing the flexoelectric coefficients (Tagantsev 1986). Experimental researches of the converse flexoelectric effect due to the inhomogeneous electric field in barium strontium was conducted by Fu *et al*. (2006). Moreover, Maranganti *et al*. (2006) developed a variation principle for dielectrics including both the strain gradient and polarization gradient effects. Then a lot of experiments have done by Ma and Cross (2001, 2002, 2006) to examine flexoelectricity quantitatively by measuring the flexoelectric coefficients of ferroelectric ceramics. In recent years, efforts have made by researchers to provide a perfect understanding of this fragile effect by investigation of experimental and theoretical results. For example, possible applications of flexoelectricity in solids has conducted by Zubko *et al*. (2013). After that, a thorough and comprehensive review of the physical fundamentals has done by Nguyen *et al*. (2013). Also, Yudin and Tagantsev (2013) presented a critical analysis of the knowledge on the flexoelectricity in common solids, excluding organic materials and liquid crystals. The influence of flexo-electricity on the electromechanical coupling behaviour of a piezoelectric nanoplate surveyed by Yang *et al*. (2015). They hired Kirchhoff plate theory and Hamilton's principle to derive their results. Also, the size dependency of the flexoelectric effect has revealed using simulation results on the electro-elastic fields. After that, Barati (2017a) examined Coupled effects of electrical polarization-strain gradient on the vibration behavior of double-layered flexoelectric nanoplates, and he succeeds in proving that flexoelectricity yields a considerable difference between his model and previous investigations on conventional piezoelectric nanoplates. More recently, Zeng *et al*. (2019) studied nonlinear vibration of piezoelectric sandwich nanoplates with functionally graded (FG) porous core under electrical load. Moreover, size-dependent nonlinear bending analysis of a flexoelectric functionally graded nano-plate under thermo-electro-mechanical loads has conducted by Ghobadi *et al*. (2019). Also, surface effects on the scale-dependent vibration behavior of flexoelectric sandwich nanobeams have evaluated by Ebrahimi *et al*. (2019b). In another attempt, Shariati *et al*. (2020) examined the vibration characteristics of flexoelectric nanobeams resting on the viscoelastic foundation and subjected to magneto-electro-viscoelastic-hygro-thermal (MEVHT) loading. As of the last example, flexoelectric and surface effects on the electromechanical behavior of graphene-based nanobeams has studied by Shingare and Kundalwal (2020). In addition, nowadays, widely utilization of sandwich plates in different industries and factories resulted in attracting scholars' attentions in this field of study (Al-Maliki *et al*. 2020, Abdulrazzaq *et al*. 2020). Such structures stiffness beside their low density in their porous type assumed as their unique privileges over single layer structures.

Studying aforementioned papers in addition to some other works (Sahoo *et al*. 2019, Patle *et al*. 2018, Dewangan *et al*. 2020, Singh *et al*. 2016a, b, Singh and Panda 2015) motivated us to derive the governing equations of motion for a size-dependent sandwich plate, including a honey-comb core and two flexoelectric face sheets based on Love-Kirchhoff's hypothesis and modified couple stress theory (MCST). The governing equations of motion are derived and solved by using Fourier series analytical method and Hamilton's principle. The results of this study investigate the effect of different boundary conditions on the vibrational behavior of sandwich flexoelectric plates. It is worthwhile mentioning that flexoelectric consideration for deriving governing equations is the most important novelty of this paper and the results of this work can be the benchmark for the future works. Moreover, such a current sandwich model with different boundary conditions has not taken into vibrational examination yet.

2. Sandwich plate modeling

As has plotted in Fig. 1, a nano sandwich plate constituted from honeycomb core patched to two same flexoelectric face sheets has considered a model to investigate the natural frequency of such structures. h_c, h_t, and h_b are the thickness of honeycomb core, top, and bottom flexoelectric face sheets, respectively, which $h = h_t+h_c+h_b$. Furthermore, θ_0 is internal calls' angle, and h_0, l_0, and t_0 are geometrical parameters of hexagonal cells. A Cartesian coordinate system (*x, y, z*) is used to describe the plate with the *z*-axis being along the thickness direction and the *x*-*y* plane sitting on the mid-plane of the plate.

The displacements of an arbitrary point in the nano sandwich plate have simulated by Love-Kirchhoff's hypothesis, for each layer, as have mentioned by Ebrahimi *et al*. (2019a) and Arshid *et al*. (2019a)

$$\tilde{u}(x,y,z,t) = u(x,y,t) - z\frac{\partial}{\partial x}w(x,y,t), \qquad (1)$$

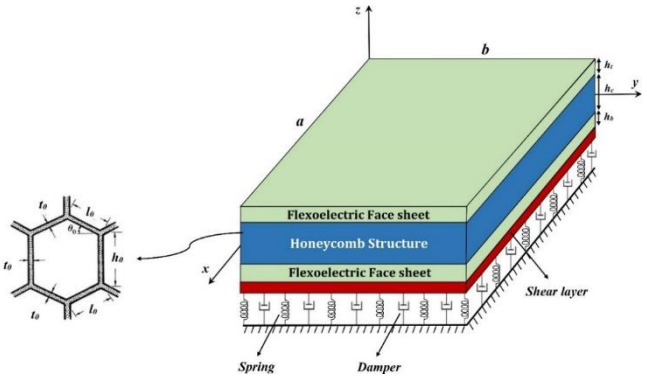

Fig. 1 Schematic figure of under evaluation honeycomb sandwich plate

$$\tilde{v}(x,y,z,t) = v(x,y,t) - z\frac{\partial}{\partial y}w(x,y,t),$$
$$\tilde{w}(x,y,z,t) = w(x,y,t), \tag{1}$$

where u, v, and w are the displacement components along the x, y, and z directions, respectively.

2.1 Honeycomb core

The honeycomb core is made of Aluminum. The strains can be obtained as (Jafari Mehrabadi 2012)

$$\varepsilon_{xx} = \frac{\partial u}{\partial x} - z\left(\frac{\partial^2 w}{\partial x^2}\right), \varepsilon_{yy} = \frac{\partial v}{\partial y} - z\left(\frac{\partial^2 w}{\partial y^2}\right),$$
$$\gamma_{xy} = \frac{\partial v}{\partial x} - 2z\left(\frac{\partial^2 w}{\partial x \partial y}\right) + \frac{\partial u}{\partial y} \tag{2}$$

The stress-Strain relationship for honeycomb core can be defined as follows (Dehshahri *et al*. 2020)

$$\begin{bmatrix} {\sigma_{xx}}^c \\ {\sigma_{yy}}^c \\ {\tau_{xy}}^c \\ {\tau_{yz}}^c \\ {\tau_{xz}}^c \end{bmatrix} = \begin{bmatrix} Q_{11} & Q_{12} & 0 & 0 & 0 \\ Q_{12} & Q_{22} & 0 & 0 & 0 \\ 0 & 0 & Q_{44} & 0 & 0 \\ 0 & 0 & 0 & Q_{55} & 0 \\ 0 & 0 & 0 & 0 & Q_{66} \end{bmatrix} \begin{bmatrix} \varepsilon_{xx} \\ \varepsilon_{yy} \\ \gamma_{xy} \\ \gamma_{yz} \\ \gamma_{xz} \end{bmatrix} \tag{3}$$

where, Q and superscript c represent elastic constant and honeycomb core, respectively. Elastic constants can be mentioned as Hebali *et al*. (2014)

$$Q_{11} = \frac{E_x + 1}{1 - \nu_{xy}\nu_{yx}}, \quad Q_{22} = \frac{E_y + 1}{1 - \nu_{xy}\nu_{yx}},$$
$$Q_{12} = Q_{21} = \frac{E_x + \nu_{yx}}{1 - \nu_{xy}\nu_{yx}}, \quad Q_{44} = G_{yz},$$
$$Q_{55} = G_{xz}, \quad Q_{66} = G_{xy} \tag{4}$$

where E, G, and v indicate elastic moduli, shear moduli and Poisson's ratio, respectively and can be defined as

$$\rho^c = \rho_{\hbar}\frac{(2+\phi_0)}{2\cos\theta_0\,(\phi_0 + \sin\theta_0)}\gamma_0$$
$$E_y = E_{\hbar}\frac{[1 - \gamma_0^2(\phi_0 \sec^2\theta_0 + \tan^2\theta_0)](\phi_0 + \sin\theta_0)}{\cos^3\theta_0}\gamma_0^3$$
$$E_x = E_{\hbar}\frac{\cos\theta_0\,(1 - \gamma_0^2\cot^2\theta_0)}{\sin^2\theta_0\,(\phi_0 + \sin\theta_0)}\gamma_0^3$$
$$\nu_{xy} = \frac{\cos^2\theta_0\,(1 - \gamma_0^2\csc^2\theta_0)}{\sin\theta_0\,(\phi_0 + \sin\theta_0)}$$
$$\nu_{yx} = \frac{(1 - \gamma_0^2(1+\phi_0)\sec^2\theta_0)\sin\theta_0\,(\phi_0 + \sin\theta_0)}{\cos^2\theta_0}$$
$$G_{xy} = E_{\hbar}\frac{(\phi_0 + \sin\theta_0)}{\phi_0^2(1+2\phi_0)\cos\theta_0}\gamma_0^3 \tag{5}$$
$$G_{xz} = G_{\hbar}\frac{\cos\theta_0}{(\phi_0 + \sin\theta_0)}\gamma_0$$
$$G_{yz} = G_{\hbar}\left[\frac{(\phi_0 + \sin\theta_0)}{(1+2\phi_0)\cos\theta_0} + \frac{(\phi_0 + 2\sin^2\theta_0)}{2(\phi_0 + \sin\theta_0)}\right]\frac{\gamma_0}{2\cos\theta_0}$$

where, ρ_h, E_h, G_h and v_h indicate density, elastic modulus, shear modulus, and Poisson's ratio of the material which honeycomb structure has made of. Also, ϕ_0 and γ_0 are internal aspect ratio and dimensionless cell thickness, respectively and can be presented as $\phi_0 = h_0/l_0$, $\gamma_0 = t_0/l_0$.

Finally, Kinetic and strain energies of nano honeycomb core can be presented as Barati (2017b)

$$K^c = \int_V \frac{1}{2}\rho_c \left[\begin{matrix}\left(\frac{\partial}{\partial t}\tilde{u}(x,y,z,t)\right)^2 + \left(\frac{\partial}{\partial t}\tilde{v}(x,y,z,t)\right)^2 \\ + \left(\frac{\partial}{\partial t}\tilde{w}(x,y,z,t)\right)^2\end{matrix}\right] dV, \tag{6}$$

$$\Gamma^c = \frac{1}{2}\int_V \left[\begin{matrix}{\sigma_{xx}}^c\varepsilon_{xx} + {\sigma_{yy}}^c\varepsilon_{yy} + {\tau_{xy}}^c\gamma_{xy} \\ + {\tau_{yz}}^c\gamma_{yz} + {\tau_{xz}}^c\gamma_{xz}\end{matrix}\right] d\,V \tag{7}$$

2.2 Flexoelectric face sheets

Based on the linear form of piezoelectricity theory, the internal energy density for flexoelectric face sheets can be defined as Zhang and Jiang (2014), Amir *et al.* (2020a)

$$U = \frac{1}{2}a_{kl}P_kP_l + \frac{1}{2}c_{ijkl}\varepsilon_{ij}\varepsilon_{kl} + d_{ijk}\varepsilon_{ij}P_k$$
$$+ \frac{1}{2}b_{ijkl}P_{i,j}P_{k,l} + f_{ijkl}u_{i,jk}P_l + e_{ijkl}\varepsilon_{ij}P_{k,l}, \tag{8}$$

where P_i, ε_{ij}, a_{kl}, c_{ijkl}, and d_{ijk} are respectively, polarization, strain, dielectric, elastic, and piezoelectric constant tensors. The polarization gradient and polarization gradient coupling tensor represent by b_{ijkl}. f_{ijkl} is the strain gradient and polarization coupling tensor. e_{ijkl} denotes the strain (Sharma *et al*. 2010). Consequently, the constitutive equations for flexoelectric face sheets can be derived as Shen and Hu (2010), Khorasani *et al*. (2020)

$$\sigma_{ij} = \frac{\partial U}{\partial \varepsilon_{ij}} = c_{ijkl}\varepsilon_{kl} + d_{ijk}P_k + e_{ijkl}P_{k,l}, \tag{9}$$

$$\sigma_{ijm} = \frac{\partial U}{\partial u_{i,jm}} = f_{ijmk}P_k, \tag{10}$$

$$E_i = \frac{\partial U}{\partial P_i} = a_{ij}P_j + d_{jki}\varepsilon_{jk} + f_{jkli}u_{j,kl}, \tag{11}$$

$$E_{ij} = \frac{\partial U}{\partial P_{i,j}} = b_{ijkl}P_{k,l} + e_{klij}\varepsilon_{kl}, \tag{12}$$

where σ_{ij}, E_i, $\sigma_{ijm,}$ and E_{ij} represent stress, electrical field, higher-order stress, and higher-order electrical field tensors, respectively. Moreover, the strain equations can be represented as follows (Ansari and Sahmani 2011)

$$\varepsilon_{xx}=\frac{\partial\tilde{u}}{\partial x},\qquad \varepsilon_{yy}=\frac{\partial\tilde{v}}{\partial y},\qquad \varepsilon_{xy}=\frac{1}{2}\left(\frac{\partial\tilde{v}}{\partial x}+\frac{\partial\tilde{u}}{\partial y}\right)$$
$$\gamma_{xxz}=\frac{\partial\varepsilon_{xx}}{\partial z},\qquad \gamma_{yyz}=\frac{\partial\varepsilon_{yy}}{\partial z},\qquad \gamma_{xyz}=\frac{\partial(2\varepsilon_{xy})}{\partial z} \tag{13}$$

Some assumptions are needed to mention the equations in a simple form as: $c_{11}=c_{1111}$, $c_{66}=c_{1212}$, $d_{31}=d_{311}$, $a_{33}=a_{3333}$ and $b_{33}=b_{3333}$, $f_{1133}=f_{2233}=f_{19}=\alpha$ (Shu *et al.* 2011). According to Fig. 1, the electric field E_i only exists in the *z*-direction (Zhao *et al.* 2007) and using Eqs. (11)-(13), the higher-order electric field E_{ij} for flexoelectric face sheets can be derived as

$$E_z=a_{33}P_z+d_{31}\left(\varepsilon_{xx}+\varepsilon_{yy}\right)+\alpha\left(\frac{\partial\varepsilon_{xx}}{\partial z}+\frac{\partial\varepsilon_{yy}}{\partial z}\right), \tag{14}$$

$$E_{zx}=b_{3133}P_{z,z}, \tag{15}$$

$$E_{zx}=b_{3133}P_{z,z}, \tag{16}$$

$$E_{zz}=b_{33}P_{z,z}-\alpha\left(\varepsilon_{xx}+\varepsilon_{yy}\right), \tag{17}$$

when the flexoelectric face sheet is under an electric potential φ across *z*-direction (across its thickness), the equilibrium equation should be satisfied as Shen and Hu (2010)

$$E_z+\frac{\partial\varphi}{\partial z}-E_{zx,x}-E_{zy,y}-E_{zz,z}=0, \tag{18}$$

where φ is the electric potential along with *z*-axis. When there is not any free electric charge on the flexoelectric face sheet, the Gauss's law can be written as Hu *et al.* (2010)

$$-k\varphi_{,zz}+P_{z,z}=0, \tag{19}$$

where $k=k_0k_b$, $k_0=8.85\times10^{-12}$ *C/V. m* is the permittivity of the air, and $k_b=6.62$ is the background permittivity of $BaTiO_3$ when its electric field is across the polarization direction (Tagantsev and Gerra 2006). Using Eqs. (14)-(19) and the electric boundary conditions $E_{ij}n_j=0$, $\varphi_{(h/2)}=V_0$ and $\varphi_{(-h/2)}=0$ for flexoelectric face sheets, and the electric potential can be derived in terms of transverse displacement, rotations of middle surface and applied voltage V_0 as Amir *et al.* (2020b)

$$\begin{aligned}&\varphi(x,y,z,t)\\&=\frac{d_{31}\left(z^2-\frac{h^2}{4}\right)\left(\frac{\partial^2w}{\partial x^2}+\frac{\partial^2w}{\partial y^2}\right)}{2(a_{33}k+1)}+\frac{V_0}{h}z+\frac{V_0}{2}+\frac{\alpha z\left(\frac{\partial^2w}{\partial x^2}+\frac{\partial^2w}{\partial y^2}\right)}{(a_{33}k+1)}\\&-\frac{\alpha h\left(e^{\lambda_2z}-\left(e^{\lambda_2z}\right)^{-1}\right)\left(\frac{\partial^2w}{\partial x^2}+\frac{\partial^2w}{\partial y^2}\right)\left(e^{\frac{\lambda_2h}{2}}-\left(e^{\frac{\lambda_2h}{2}}\right)^{-1}\right)^{-1}}{2(a_{33}k+1)}\\&+\frac{b_{33}kd_{31}}{(a_{33}k+1)^2}\left(1-\frac{e^{\lambda_2z}+\left(e^{\lambda_2z}\right)^{-1}}{e^{\frac{\lambda_2h}{2}}+\left(e^{\frac{\lambda_2h}{2}}\right)^{-1}}\right)+\left(\frac{\partial^2w}{\partial x^2}+\frac{\partial^2w}{\partial y^2}\right)\\&-\frac{\alpha}{(a_{33}k+1)}\left(1-\frac{e^{\lambda_2z}+\left(e^{\lambda_2z}\right)^{-1}}{e^{\frac{\lambda_2h}{2}}+\left(e^{\frac{\lambda_2h}{2}}\right)^{-1}}\right)\left(\frac{\partial u}{\partial x}+\frac{\partial v}{\partial y}\right),\end{aligned} \tag{20}$$

where $\lambda_2=\sqrt{1+ka_{33}/kb_{33}}$. Using Eqs. (23) and (24) the polarization is

$$\begin{aligned}P_z=&2\frac{kd_{31}z\left(\frac{\partial^2w}{\partial x^2}+\frac{\partial^2w}{\partial y^2}\right)}{2(a_{33}k+1)}+\frac{kV_0}{h}+\frac{k\alpha\left(\frac{\partial^2w}{\partial x^2}+\frac{\partial^2w}{\partial y^2}\right)}{(a_{33}k+1)}\\&-\frac{b_{33}k^2d_{31}\left(e^{\lambda_2z}\lambda_2-\frac{\lambda_2}{e^{\lambda_2z}}\right)\left(\frac{\partial^2w}{\partial x^2}+\frac{\partial^2w}{\partial y^2}\right)\left(e^{\frac{\lambda_2h}{2}}+\left(e^{\frac{\lambda_2h}{2}}\right)^{-1}\right)^{-1}}{(a_{33}k+1)^2}\\&-\frac{k\alpha h\left(e^{\lambda_2z}\lambda_2+\frac{\lambda_2}{e^{\lambda_2z}}\right)\left(\frac{\partial^2w}{\partial x^2}+\frac{\partial^2w}{\partial y^2}\right)\left(e^{\frac{\lambda_2h}{2}}-\left(e^{\frac{\lambda_2h}{2}}\right)^{-1}\right)^{-1}}{2(a_{33}k+1)}\\&+\frac{k\alpha\left(e^{\lambda_2z}\lambda_2-\frac{\lambda_2}{e^{\lambda_2z}}\right)\left(\frac{\partial u}{\partial x}+\frac{\partial v}{\partial y}\right)\left(e^{\frac{\lambda_2h}{2}}+\left(e^{\frac{\lambda_2h}{2}}\right)^{-1}\right)^{-1}}{(a_{33}k+1)}.\end{aligned} \tag{21}$$

Substitution of Eq. (21) into Eqs. (14) and (17), respectively, the electrical field in the *z*-direction (E_z) and higher-order electric field (E_{zz}) for top and bottom flexoelectric face sheets can be obtained as

$$\begin{aligned}E_z=&a_{33}k(2\frac{d_{31}z\left(+\frac{\partial^2w}{\partial x^2}+\frac{\partial^2w}{\partial y^2}\right)}{2(a_{33}k+1)}+\frac{V_0}{h}+\frac{\alpha\left(+\frac{\partial^2w}{\partial x^2}+\frac{\partial^2w}{\partial y^2}\right)}{(a_{33}k+1)}\\&-\frac{\alpha h\left(e^{\lambda_2z}\lambda_2+\frac{\lambda_2}{e^{\lambda_2z}}\right)\left(+\frac{\partial^2w}{\partial x^2}+\frac{\partial^2w}{\partial y^2}\right)\left(e^{\frac{\lambda_2h}{2}}-\left(e^{\frac{\lambda_2h}{2}}\right)^{-1}\right)^{-1}}{2(a_{33}k+1)}\\&-\frac{b_{33}kd_{31}\left(e^{\lambda_2z}\lambda_2-\frac{\lambda_2}{e^{\lambda_2z}}\right)\left(+\frac{\partial^2w}{\partial x^2}+\frac{\partial^2w}{\partial y^2}\right)\left(e^{\frac{\lambda_2h}{2}}+\left(e^{\frac{\lambda_2h}{2}}\right)^{-1}\right)^{-1}}{(a_{33}k+1)^2}\\&+\frac{\alpha\left(e^{\lambda_2z}\lambda_2-\frac{\lambda_2}{e^{\lambda_2z}}\right)\left(\frac{\partial u}{\partial x}+\frac{\partial v}{\partial y}\right)\left(e^{\frac{\lambda_2h}{2}}+\left(e^{\frac{\lambda_2h}{2}}\right)^{-1}\right)^{-1}}{(a_{33}k+1)})\\&+d_{31}\left(\frac{\partial u}{\partial x}+\frac{\partial v}{\partial y}-z\frac{\partial^2w}{\partial x^2}-z\frac{\partial^2w}{\partial y^2}\right)+k_s\alpha\left(-\frac{\partial^2w}{\partial x^2}-\frac{\partial^2w}{\partial y^2}\right),\end{aligned} \tag{22}$$

$$\begin{aligned}E_{zz}=&b_{33}k(\frac{d_{31}\left(\frac{\partial^2w}{\partial x^2}+\frac{\partial^2w}{\partial y^2}\right)}{(a_{33}k+1)}\\&-\frac{\alpha h}{(a_{33}k+1)}\left(e^{\lambda_2z}{\lambda_2}^2-\frac{{\lambda_2}^2}{e^{\lambda_2z}}\right)\left(\frac{\partial^2w}{\partial x^2}+\frac{\partial^2w}{\partial y^2}\right)\left(e^{\frac{\lambda_2h}{2}}-\left(e^{\frac{\lambda_2h}{2}}\right)^{-1}\right)^{-1}\\&-\frac{b_{33}kd_{31}}{(a_{33}k+1)^2}\left(2e^{\lambda_2z}{\lambda_2}^2+\frac{2{\lambda_2}^2}{e^{\lambda_2z}}\right)\left(\frac{\partial^2w}{\partial x^2}+\frac{\partial^2w}{\partial y^2}\right)\left(e^{\frac{\lambda_2h}{2}}+\left(e^{\frac{\lambda_2h}{2}}\right)^{-1}\right)^{-1}\\&+\frac{\alpha}{(a_{33}k+1)}\left(2e^{\lambda_2z}{\lambda_2}^2+\frac{2{\lambda_2}^2}{e^{\lambda_2z}}\right)\left(\frac{\partial u}{\partial x}+\frac{\partial v}{\partial y}\right)\left(e^{\frac{\lambda_2h}{2}}+\left(e^{\frac{\lambda_2h}{2}}\right)^{-1}\right)^{-1})\\&-\alpha\left(\frac{\partial u}{\partial x}-z\frac{\partial^2w}{\partial x^2}+\frac{\partial v}{\partial y}-z\frac{\partial^2w}{\partial y^2}\right).\end{aligned} \tag{23}$$

After the derivation of electric field terms, the stresses of flexoelectric face sheets can be determined from the constitutive as follows

$$\begin{aligned}\begin{Bmatrix}\sigma_{xx}\\\sigma_{yy}\\\sigma_{xy}\\\tau_{xxz}\\\tau_{yyz}\\\tau_{xyz}\end{Bmatrix}=&\begin{bmatrix}c_{11}&c_{12}&0&0&0&0\\c_{21}&c_{22}&0&0&0&0\\0&0&c_{66}&0&0&0\\0&0&0&0&0&0\\0&0&0&0&0&0\\0&0&0&0&0&0\end{bmatrix}\begin{Bmatrix}\varepsilon_{xx}\\\varepsilon_{yy}\\\gamma_{xy}\\\gamma_{xxz}\\\gamma_{yyz}\\\gamma_{xyz}\end{Bmatrix}\\&+\begin{bmatrix}d_{31}k&k_s\alpha k\\d_{32}k&k_s\alpha k\\0&0\\k_s\alpha k&0\\k_s\alpha k&0\\0&0\end{bmatrix}\begin{Bmatrix}\frac{\partial\varphi}{\partial z}\\-\frac{\partial^2\varphi}{\partial z^2}\end{Bmatrix},\end{aligned} \tag{24}$$

in Eq. (24), ks is a shear correction factor which is equal to 5/6.

At the end, using Eqs. (1), (13) and (20)-(24) the kinetic

and strain energy of flexoelectric face sheets can be defined as Liu *et al*. (2012), Amir *et al*. (2020c)

$$K^f = \int_V \frac{1}{2}\rho_f \begin{bmatrix} \left(\frac{\partial}{\partial t}\tilde{u}(x,y,z,t)\right)^2 + \left(\frac{\partial}{\partial t}\tilde{v}(x,y,z,t)\right)^2 \\ + \left(\frac{\partial}{\partial t}\tilde{w}(x,y,z,t)\right)^2 \end{bmatrix} dV, \quad (25)$$

$$\Gamma^f = \frac{1}{2}\int_V \begin{pmatrix} \sigma_{xx}\,\varepsilon_{xx} + \sigma_{yy}\,\varepsilon_{yy} + 2\sigma_{xy}\,\varepsilon_{yy} \\ + \tau_{yyz}\,\gamma_{yyz} + \tau_{xyz}\,\gamma_{xyz} + E_z p_z \\ + E_{zz}\frac{\partial}{\partial z}p_z - k\left(\frac{\partial}{\partial z}\varphi(x,y,z,t)\right)^2 \\ + p_z\frac{\partial}{\partial z}\varphi(x,y,z,t) \end{pmatrix} dV, \quad (26)$$

3. Governing equations of motion

Hamilton's principle has used to extract the governing equations as follows (Arshid and Khorshidvand 2018, Salari *et al*. 2019)

$$\delta\Pi = \delta\int_{t_1}^{t_2}(\Gamma^{c,f,m} - K^{c,f} - \Sigma)dt = 0, \quad (27)$$

in which Γ, *K*, and ∑ represent strain energy, kinetic energy, and external work, respectively. Superscripts *c*, *f*, and *m* are, respectively, representative of the words, core, face sheets, and *MCST*.

MCST has utilized to consider the size effect of the aforementioned sandwich plate.

The equation of strain energy is presented as follows (Akbas 2018, Arshid *et al.* 2020a)

$$\Gamma^m = \int_V \frac{1}{2}\begin{bmatrix} m_{xx}\chi_{xx} + m_{yy}\chi_{yy} + m_{xy}\chi_{xy} \\ + m_{xz}\chi_{xz} + m_{yz}\chi_{yz} \end{bmatrix} dV, \quad (28)$$

where m_{lk} and χ_{lk} are stress and symmetric curvature tensor. As another expression, m_{lk} is a part of couple stress tensor, which is ignorable in macro-scale whereas, plays a crucial role in nano-scale. Furthermore, the superscript *m* denotes *MCST*. m_{lk} and χ_{lk} can be presented as (Arshid *et al*. 2019b)

$$\begin{aligned} \chi_{xx} &= \frac{\partial^2 w}{\partial y \partial x}, & \chi_{yy} &= -\frac{\partial^2 w}{\partial y \partial x}, \\ \chi_{xy} &= \frac{1}{2}\left(\frac{\partial^2 w}{\partial y^2} - \frac{\partial^2 w}{\partial x^2}\right), & \chi_{xz} &= \frac{1}{4}\left(\frac{\partial^2 v}{\partial x^2} - \frac{\partial^2 u}{\partial y \partial x}\right), \\ \chi_{yz} &= \frac{1}{4}\left(\frac{\partial^2 v}{\partial y \partial x} - \frac{\partial^2 u}{\partial y^2}\right) \end{aligned} \quad (29)$$

$$m_{lk} = 2{L_m}^2 G\chi_{lk}, \quad (30)$$

where L_m is the material length scale parameter, and *G* assumes to be equal to Q_{66}.

Substituting Eqs. (29) and (30) to Eq. (28) the strain energy due to *MCST* can be obtained.

Visco-Pasternak foundation is capable of considering normal and transverse shear loads. The force applied on the sandwich plate due to the visco-Pasternak foundation can be determined as Arshid *et al.* (2021), Zenkour (2016)

$$\begin{aligned} F^{Visco-Pasternak foundation} &= K_w w(x,y,t) \\ -K_g\frac{\partial^2 w(x,y,t)}{\partial x^2} - K_g\frac{\partial^2 w(x,y,t)}{\partial y^2} + C_d\frac{\partial w(x,y,t)}{\partial t}, \end{aligned} \quad (31)$$

where K_w is the Winkler spring coefficient, and K_g is shear layer parameters in *x* and *y* directions, respectively. Also, C_d is damping constant. Therefore, the work of the elastic medium is as follows (Arshid *et al*. 2020b, Amir *et al.* 2020d)

$$\Sigma = \frac{1}{2}\int_A F^{Visco-Pasternak foundation} w dA, \quad (32)$$

Substitution of Eqs. (6)-(7), (25)-(26), (28) and (32) into Eq. (27), the equations of motion can be obtained by setting the coefficients δu, δv, $\delta\Phi$, and δw equal to zero (Amir *et al.* 2019).

4. Analytical solution procedure

In the case of considering different boundary conditions and in order to separate variables related to space and time for the sandwich plate, the displacement components can be defined as Bendaho *et al.* (2019), Khorasani *et al.* (2021)

$$\begin{aligned} u(x,y,t) &= \sum_{m=1}^{M}\sum_{n=1}^{N} U_{mn}\frac{dX_m(x)}{dx}Y_n(y)e^{i\omega_{mn}t} \\ v(x,y,t) &= \sum_{m=1}^{M}\sum_{n=1}^{N} V_{mn}\frac{dY_n(y)}{dy}X_m(x)e^{i\omega_{mn}t} \\ w(x,y,t) &= \sum_{m=1}^{M}\sum_{n=1}^{N} W_{mn}X_m(x)Y_n(y)e^{i\omega_{mn}t} \\ \Phi(x,y,t) &= \sum_{m=1}^{M}\sum_{n=1}^{N} \Phi_{mn}X_m(x)Y_n(y)e^{i\omega_{mn}t} \end{aligned} \quad (33)$$

in which *X*(*x*) and *Y*(*y*) are hired to switch among different boundary conditions and define as follow

$$\begin{aligned} X_m(x) &= sin(\varpi_m x) + \zeta_m\, cos(\varpi_m x) \\ &+\eta_m\, sinh(\varpi_m x) + \xi_m\, cosh(\varpi_m x) \\ Y_n(x) &= sin(\varpi_n y) + \zeta_n\, cos(\varpi_n y) \\ &+\eta_n\, sinh(\varpi_n y) + \xi_n\, cosh(\varpi_n y) \end{aligned} \quad (34)$$

All constants related to these equations for different boundary conditions are listed in Table 1 as below.

U_{mn}, V_{mn}, W_{mn}, and Φ_{mn} are unknown coefficients of each mode, and ω_{mn} represents the natural frequency. The mode numbers along *x* and *y* directions are, respectively, *m* and *n*. Eventually, the equations of motion can be defined as a matric form as Arshid *et al.* (2020c)

$$\begin{aligned} &[A]_{4\times4}[U_{mn} \quad V_{mn} \quad W_{mn} \quad \Phi_{mn}]^{Transverse} \\ &= [zero]_{4\times1} \end{aligned} \quad (35)$$

The arrays of matric [*A*] are obtained by substituting Eq. (33) into the governing equation of motion which have obtained in the previous section.

5. Numerical results and discussions

The effect of different variables' change on the non-

Table 1 Different boundary condition constants

B.C.	SSSS	SSCS	CSCS	FCFC	FCCS	CCCC
ϖ_m	$\frac{m\pi}{a}$	$\frac{m\pi}{a}$	$\frac{(4m+1)\pi}{4a}$	$\frac{(2m-1)\pi}{4a}$	$\frac{(2m-1)\pi}{4a}$	$\frac{(2m+1)\pi}{2a}$
ϖ_n	$\frac{n\pi}{b}$	$\frac{(4n+1)\pi}{4b}$	$\frac{(4n+1)\pi}{4b}$	$\frac{(2n-1)\pi}{4b}$	$\frac{(4n+1)\pi}{4b}$	$\frac{(2n+1)\pi}{2b}$
ζ_m	0	0	0	$\frac{-(sin(\varpi_m a)+sinh(\varpi_m a))}{cos(\varpi_m a)+cosh(\varpi_m a)}$	$\frac{-(sin(\varpi_m a)+sinh(\varpi_m a))}{cos(\varpi_m a)+cosh(\varpi_m a)}$	$\frac{-(sin(\varpi_m a)+sinh(\varpi_m a))}{cos(\varpi_m a)+cosh(\varpi_m a)}$
ζ_n	0	0	0	$\frac{-(sin(\varpi_n b)+sinh(\varpi_n b))}{cos(\varpi_n b)+cosh(\varpi_n b)}$	0	$\frac{-(sin(\varpi_n b)-sinh(\varpi_n b))}{cos(\varpi_n b)-cosh(\varpi_n b)}$
η_m	0	0	$\frac{-\sin\varpi_m a}{sinh\varpi_m a}$	-1	-1	-1
η_n	0	$\frac{-\sin\varpi_n b}{sinh\varpi_n b}$	$\frac{-\sin\varpi_n b}{sinh\varpi_n b}$	-1	$\frac{-\sin\varpi_n b}{sinh\varpi_n b}$	-1
ξ_m	0	0	0	$-\zeta_m$	$-\zeta_m$	$-\zeta_m$
ξ_n	0	0	0	$-\zeta_n$	0	$-\zeta_n$

Table 2 Mechanical properties of Aluminum honeycomb core (Nakamoto *et al*. 2009)

ρ_h (kg/m^3)	E_h (GPa)	G_h (GPa)	ν_h
2700	70	26	0.33

Table 3 Mechanical properties of $BaTiO_3$ flexoelectric face sheets (Zhang and Jiang 2014, Zhang *et al*. 2014)

ρ_f (kg/m^3)	$c_{11}=c_{22}$ (GPa)	$c_{12}=c_{21}$ (GPa)	c_{66} (GPa)
6020	167.55	78.15	44.7
a_{33} (V.m/C)	b_{33} (J.m^3/C^2)	$d_{31}=d_{32}$ (V/m)	α (V)
0.79×10^8	1×10^{-9}	3.5×10^8	10

dimensional natural frequency of the abovementioned structure has plotted in different figures in this section. Natural frequencies have transformed into non-dimensional type as $\bar{\omega}=\omega_0 h_f\sqrt{\rho_f/C_{11}}$.

The material properties of Aluminium as nano honeycomb core and $BaTiO_3$ as flexoelectric face sheets have presented in Tables 2 and 3, respectively (Nakamoto *et al*. 2009, Zhang and Jiang 2014, Zhang *et al*. 2014).

The geometrical and mechanical properties of the sandwich plate are considered as follow

$$h_c=2(nm),\quad h_f=0.1(nm),\quad a=b=10h,$$
$$K_w=10^9\left(\frac{N}{m^3}\right),\quad K_g=10^9\left(\frac{N}{m}\right),$$
$$C_d=10^{28}\left(\frac{kg}{s}\right),\quad \theta_0=\frac{\pi}{4},\quad \phi_0=1,$$
$$\gamma_0=0.1,\quad L_m=15e-6,\quad \alpha=8.3$$

In order to guaranty the reliability of the results of this research, using MCST, the effects of length to thickness ratio (a/h), different material gradient index (n) and h/L_m on the non-dimensional natural frequency of a single-layer FGM rectangular plate in micro dimension compared with Thai and Choi (2013) and He *et al.* (2015) in Table 4.

Finally, using Table 4, it is clear that a good agreement exists among the results of the present study and Thai and Choi (2013), He *et al*. (2015).

Table 4 Comparison among the results of FGM micro rectangular plate in the present study and previous ones

a/h	h/L_m	Ref.	$n=0$	$n=1$
5	5	Thai and Choi (2013)	5.7797	5.3239
		He *et al*. (2015)	5.8439	5.3749
		Present	5.7571	5.4132
	2.5	Thai and Choi (2013)	6.7996	6.4600
		He *et al*. (2015)	7.0322	6.6512
		Present	6.6026	6.5810
	1	Thai and Choi (2013)	11.1311	11.0451
		He *et al*. (2015)	12.4874	12.3118
		Present	11.1313	11.1078
10	5	Thai and Choi (2013)	6.3559	5.7518
		He *et al*. (2015)	6.3770	5.7676
		Present	6.3247	5.7982
	2.5	Thai and Choi (2013)	7.4807	6.9920
		He *et al*. (2015)	7.5590	7.0532
		Present	7.4003	7.1379
	1	Thai and Choi (2013)	12.6360	12.4128
		He *et al*. (2015)	13.1220	12.8483
		Present	12.6221	12.4510

The dimensionless natural frequency of nano sandwich structure with honeycomb core versus aspect ratio (a/h) for different boundary conditions has shown in Fig. 2. As it is evident, the square basis provides less frequency in comparison with a rectangular basis in each boundary condition, which means a more stable nano sandwich structure. Also, among different boundary conditions, *SSSS* and *CCCC* have the lowest and highest natural frequency, respectively.

Fig. 3 displays different curvatures related to natural frequency against width to thickness ratio of under examination structure in different mode numbers and

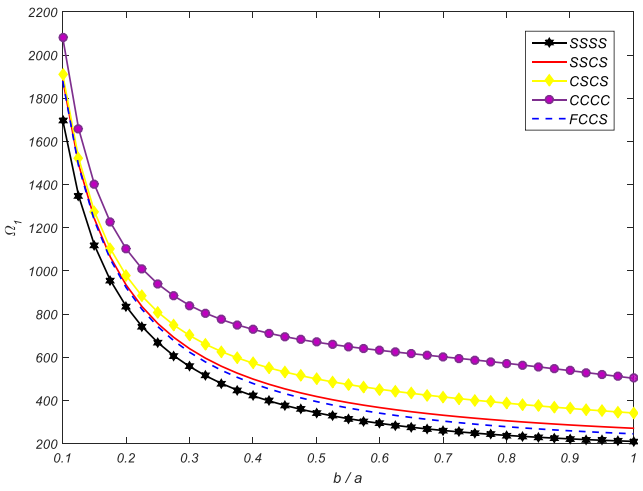

Fig. 2 Variations of dimensionless natural frequency versus aspect ratio (b/a) for different boundary conditions

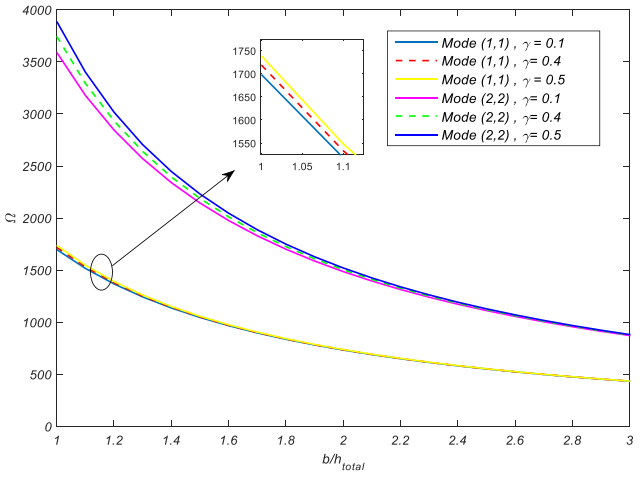

Fig. 3 Variations of non-dimensional natural frequency versus width to thickness ratio (b/h) for different mode numbers

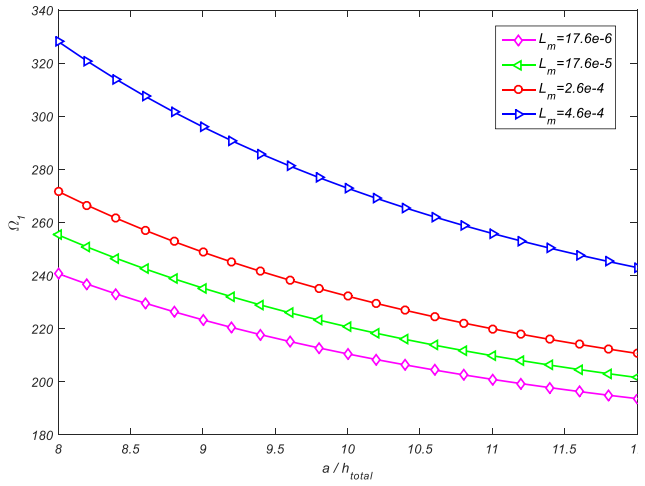

Fig. 4 Variations of dimensionless natural frequency versus length to thickness ratio (a/h) for different length scale parameters

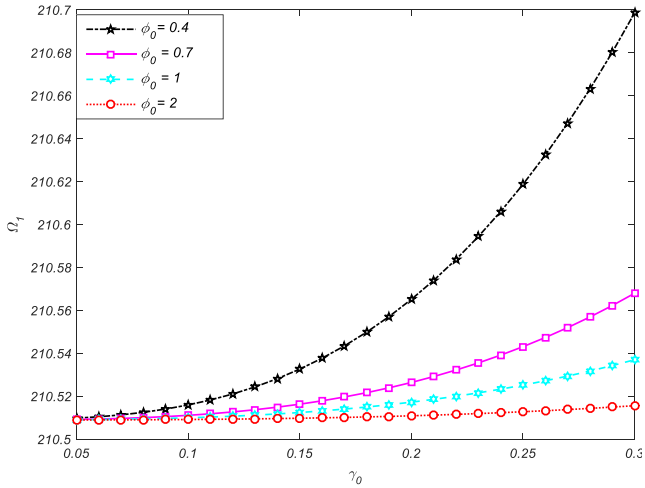

Fig. 5 Variations of non-dimensional natural frequency versus γ_0 and ϕ_0

gamma allocations. By (b/a) enhancement, dimensionless natural frequency reduces continuously in each mode number. Using this figure, it can be concluded that the stiffness of such structures increases when higher values of gamma become used in equations.

Fig. 4 has presented to evaluate the effect of length scale parameter variation on the non-dimensional natural frequency of the current model versus a considered length to height ration (a/h). As a physical interpretation, it should be mentioned that the value of the length scale parameter has a direct relationship with sandwich structure stability. Therefore, higher values of (L_m) result in higher natural frequency gaining.

The effect of internal aspect ratio ϕ_0 and dimensionless cell thickness γ_0 on the natural frequency of the current sandwich plate has investigated in Fig. 5. As it is clear, larger magnitudes of γ_0 lead to an increase in system stability. On the other hand, by increasing the magnitude of ϕ_0, natural frequency reduces dramatically, which means lower stiffness and stronger flexibility. In order to gain this figure, the internal cells' angle assumed to be 45°.

Fig. 6 implies that thicker honeycomb core causes more natural frequency. Furthermore, larger magnitudes of damper constants increase the flexibility of the system. As another expression, by elevating the value of damper constant, stiffness of the whole nano sandwich structure reduces so, the natural frequency falls down. Moreover, in the case of same C_d using, the broader basis of under evaluating model provides less natural frequency in each honeycomb core thickness.

According to the results plotted in Fig. 7, the influence of internal cells' angle variations of honeycomb core on the natural frequency of sandwich structure have examined. As the figure illustrates, the enhancement of θ_0 leads to natural frequency enlargement. Moreover, Fig. 7 illustrates increasing flexoelectric coefficient, causes dimensionless natural frequency reduction, which leads to stiffness enhancement in each selected boundary condition.

Considering Fig. 8 as a witness, the whole under the examination system goes toward less stable behavior as the thickness of face sheets increases in each mode. As another important mentioning consequence, it should be noted that,

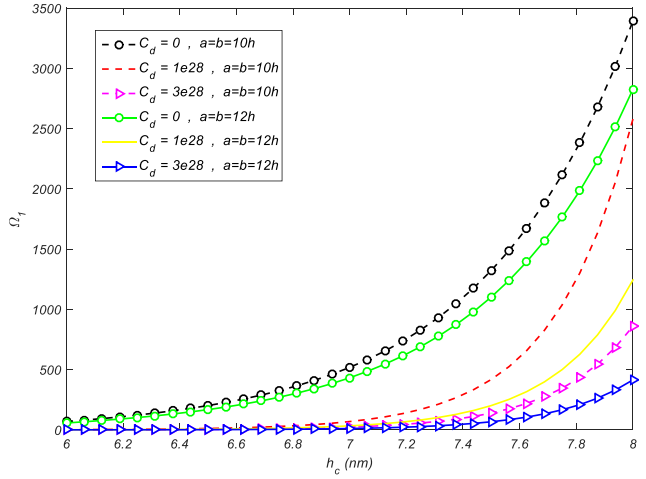

Fig. 6 Dimensionless natural frequency versus thickness of honeycomb core (h_c) for different damper constants C_d

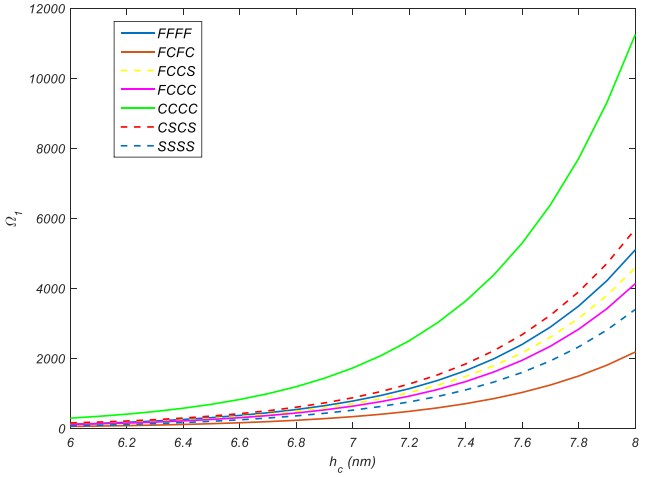

Fig. 9 Influence of core thickness and different boundary conditions on first mode dimensionless natural frequency

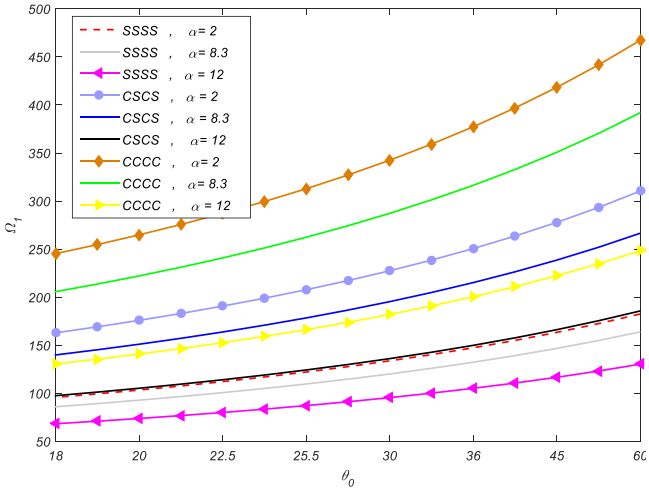

Fig. 7 Variations of non-dimensional natural frequency versus internal cells' angle θ_0 for different boundary conditions and different flexoelectric coefficients α

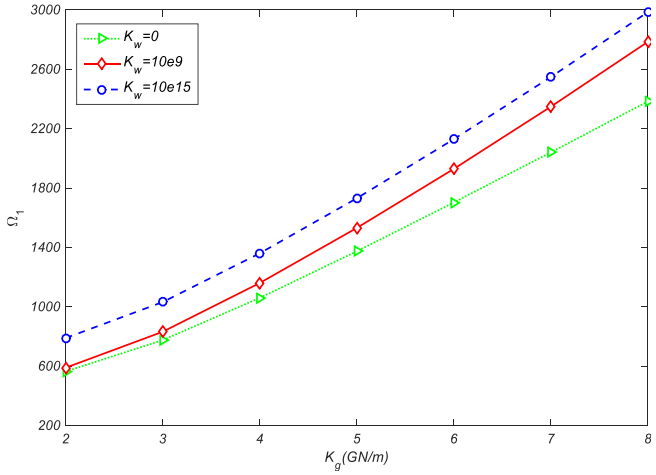

Fig. 10 Dimensionless natural frequency versus foundation modulus

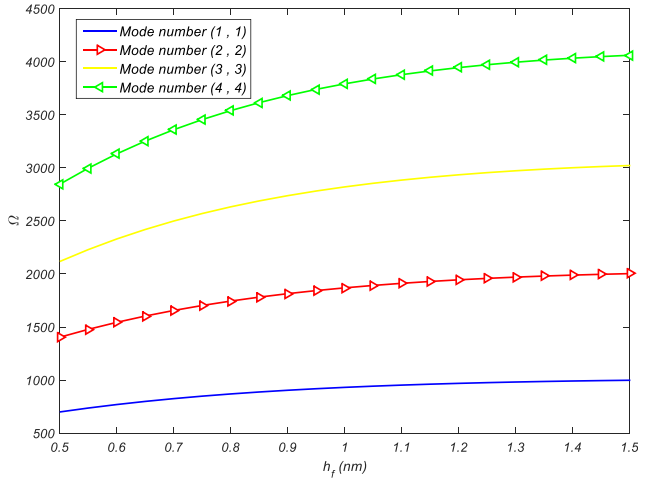

Fig. 8 Effect of face sheets' thickness on non-dimensional natural frequency versus different mode numbers

in higher mode numbers, the variations of natural frequency are more face sheets' thickness dependent. It shows, with a low magnitude of change in (h_f), natural frequency changes more obviously.

Fig. 9 proves the role of honeycomb core thickness and different boundary conditions on the dimensionless natural frequency of the current nano sandwich model with flexoelectric face sheets and honeycomb core. As it is visible, the same as flexoelectric face sheets thickness, honeycomb core thickness enhancement results in natural frequency increasing. This effect is more touchable in higher values of core thickness. Moreover, the highest and lowest stability of the aforementioned structure become provided by *CCCC* and *FCFC* as system's boundary condition, respectively.

Finally, the role of the vicso-Pasternak foundation in non-dimensional natural frequency of the abovementioned sandwich structure has taken into examination in Fig. 10. By increasing the Winkler and Pasternak parameters, the stiffness and consequently natural frequency increases, which means nailing to the less flexible sandwich structure.

6. Conclusions

Using Love-Kirchhoff's hypothesis and MCST, the size-dependent vibrational behavior of a sandwich plate, including honeycomb core and flexoelectric face sheets, examined in the current study. For governing equations elicitation, Hamilton's principle and Fourier series analytical method have hired. Current research illustrates a high sandwich structure's vibration dependency on the flexoelectric parameter on the nano-scale. Moreover, in this paper, a tremendous effort has done to examine the effect of different parameter changes on the dimensionless natural frequency of such honeycomb sandwich structures. Some worthwhile marking results have listed below as:

•Thicker layers of flexoelectric face sheets and honeycomb core lead to the stiffer sandwich plate, and consequently, the natural frequency increases by different layers' thickness increasing.

•The sensitivity of dimensionless natural frequency to length scale and flexoelectric parameters has proved in this paper. Natural frequency increases with length scale parameter enhancement and flexoelectric parameter reduction.

•It has revealed that among various boundary conditions, *CCCC* always provides less flexibility and, consequently, the highest frequency for such sandwich structures.

•Among different geometrical parameters of honeycomb core, γ_0 and θ_0 have direct and ϕ_0 has an indirect relationship with the dimensionless natural frequency of the system.

These results can help to design and manufacturing of smart systems more precisely. The aim of this work is too broad the borders of science related to structures with flexoelectric effects consideration.

References

Abdulrazzaq, M.A., Fenjan, R.M., Ahmed, R.A. and Faleh, N.M. (2020), "Thermal buckling of nonlocal clamped exponentially graded plate according to a secant function based refined theory", *Steel. Compos. Struct., Int. J.*, **35**(1), 147-157. https://doi.org/10.12989/scs.2020.35.1.149.

Akbas, S.D. (2018), "Forced vibration analysis of cracked functionally graded microbeams", *Adv. Nano. Res., Int. J.*, **6**(1), 39-55. https://doi.org/10.12989/anr.2018.6.1.039.

Al-Maliki, A.F.H., Ahmed, R.A., Moustafa, N.M. and Faleh, N.M. (2020), "Finite element based modeling and thermal dynamic analysis of functionally graded graphene reinforced beams", *Adv. Computat. Des., Int. J.*, **5**(2), 177-193. https://doi.org/10.12989/acd.2020.5.2.177.

Amir, S., Khorasani, M. and BabaAkbar-Zarei, H. (2020a), "Buckling analysis of nanocomposite sandwich plates with piezoelectric face sheets based on flexoelectricity and first-order shear deformation theory", *J. Sandw. Struct. Mater.*, **22**(7), 2186-2209. https://doi.org/10.1177/1099636218795385.

Amir, S., BabaAkbar-Zarei, H. and Khorasani, M. (2020b), "Flexoelectric vibration analysis of nanocomposite sandwich plates", *Mech. Based Des. Struct. Mach.*, **48**(2), 146-163. https://doi.org/10.1080/15397734.2019.1624175.

Amir, S., Arshid, E., Khoddami Maraghi, Z., Loghman, A. and Ghorbanpour Arani, A. (2020c), "Vibration analysis of magnetorheological fluid circular sandwich plates with magnetostrictive facesheets exposed to monotonic magnetic field located on visco-Pasternak substrate", *J. Vib. Control*, **26**(17-18), 1523-1537. https://doi.org/10.1177/1077546319899203.

Amir, S., Arshid, E. and Khoddami Maraghi, Z. (2020d), "Free vibration analysis of magneto-rheological smart annular three-layered plates subjected to magnetic field in viscoelastic medium", *Smart Struct. Syst., Int. J.*, **25**(5), 581-592. https://doi.org/https://doi.org/10.12989/sss.2020.25.5.581.

Amir, S., Soleimani-Javid, Z. and Arshid, E. (2019), "Size-dependent free vibration of sandwich micro beam with porous core subjected to thermal load based on SSDBT", *ZAMM - J. Appl. Math. Mech. / Zeitschrift Für Angewandte Mathematik Und Mechanik*, **99**(9). https://doi.org/10.1002/zamm.201800334.

Ansari, R. and Sahmani, S. (2011), "Surface stress effects on the free vibration behavior of nanoplates", *Int. J. Eng. Sci.*, **49**(11), 1204-1215. https://doi.org/10.1016/j.ijengsci.2011.06.005.

Arshid, E. and Khorshidvand, A.R. (2018), "Thin-Walled Structures Free vibration analysis of saturated porous FG circular plates integrated with piezoelectric actuators via differential quadrature method", *Thin Wall. Struct.*, **125**(January), 220-233. https://doi.org/10.1016/j.tws.2018.01.007.

Arshid, E., Amir, S. and Loghman, A. (2020a), "Static and dynamic analyses of FG-GNPs reinforced porous nanocomposite annular micro-plates based on MSGT", *Int. J. Mech. Sci.*, **180**, 105656. https://doi.org/10.1016/j.ijmecsci.2020.105656.

Arshid, E., Amir, S. and Loghman, A. (2020b), "Bending and buckling behaviors of heterogeneous temperature-dependent micro annular/circular porous sandwich plates integrated by FGPEM nano-Composite layers", *J. Sandw. Struct. Mater.*, 109963622095502. https://doi.org/10.1177/1099636220955027.

Arshid, H., Khorasani, M., Soleimani-Javid, Z., Dimitri, R. and Tornabene, F. (2020c), "Quasi-3D Hyperbolic Shear Deformation Theory for the Free Vibration Study of Honeycomb Microplates with Graphene Nanoplatelets-Reinforced Epoxy Skins", *Molecules*, **25**(21), 5085. https://doi.org/10.3390/molecules25215085.

Arshid, E., Arshid, H., Amir, S. and Mousavi, S.B. (2021), "Free vibration and buckling analyses of FG porous sandwich curved microbeams in thermal environment under magnetic field based on modified couple stress theory", *Arch. Civil. Mech. Eng.*, **21**(1), 6. https://doi.org/10.1007/s43452-020-00150-x.

Arshid, E., Khorshidvand, A.R. and Khorsandijou, S.M. (2019a), "The effect of porosity on free vibration of SPFG circular plates resting on visco-Pasternak elastic foundation based on CPT, FSDT and TSDT", *Struct. Eng. Mech., Int. J.*, **70**(1), 97-112. https://doi.org/10.1177/1464420719832626.

Arshid, E., Kiani, A. and Amir, S. (2019b), "Magneto-electro-elastic vibration of moderately thick FG annular plates subjected to multi physical loads in thermal environment using GDQ method by considering neutral surface", *Proceedings of the Institution of Mechanical Engineers, Part L: Journal of Materials: Design and Applications*, **233**(10), 2140-2159. https://doi.org/10.1177/1464420719832626.

Barati, M.R. (2017a), "Coupled effects of electrical polarization-strain gradient on vibration behavior of double-layered flexoelectric nanoplates", *Smart Struct. Syst., Int. J.*, **20**(5), 573-581. https://doi.org/10.12989/sss.2017.20.5.573.

Barati, M.R. (2017b), "Nonlocal-strain gradient forced vibration analysis of metal foam nanoplates with uniform and graded", *Adv. Nano. Res., Int. J.*, **5**(4), 393-414. https://doi.org/10.12989/anr.2017.5.4.393.

Bendaho, B., Belabed, Z., Bourada, M., Benatta, M.A., Bourada,

F. and Tounsi, A. (2019), "Assessment of new 2D and quasi-3D nonlocal theories for free vibration analysis of size-dependent functionally graded (FG) nanoplates", *Adv. Nano. Res., Int. J.*, **7**(4), 277-292. https://doi.org/10.12989/anr.2019.7.4.277.

Bisen, H.B., Hirwani, C.K., Satankar, R.K., Panda, S.K., Mehar, K. and Patel, B. (2020), "Numerical study of frequency and deflection responses of natural fiber (Luffa) reinforced polymer composite and experimental validation", *J. Natural Fibers*, **17**(4), 505-519. https://doi.org/10.1080/15440478.2018.1503129.

Dewangan, H.C., Sharma, N., Hirwani, C.K. and Panda, S.K. (2020), "Numerical eigenfrequency and experimental verification of variable cutout (square/rectangular) borne layered glass/epoxy flat/curved panel structure", *Mech. Based Des. Struct.*, 1-18. https://doi.org/10.1080/15397734.2020.1759432.

Ebrahimi, F., Dabbagh, A., Tornabene, F. and Civalek, O. (2019a), "Hygro-thermal effects on wave dispersion responses of magnetostrictive sandwich nanoplates", *Adv. Nano. Res., Int. J.*, **7**(3), 157-167. https://doi.org/10.12989/anr.2019.7.3.157.

Ebrahimi, F., Karimiasl, M., Civalek, Ö. and Vinyas, M. (2019b), "Surface effects on scale-dependent vibration behavior of flexoelectric sandwich nanobeams", *Adv. Nano. Res., Int. J.*, **7**(2), 77-88. https://doi.org/10.12989/anr.2019.7.2.077.

Fu, J.Y., Zhu, W., Li, N. and Cross, L.E. (2006), "Experimental studies of the converse flexoelectric effect induced by inhomogeneous electric field in a barium strontium titanate composition", *J. Appl. Phys.*, **100**(2). https://doi.org/10.1063/1.2219990.

Ghobadi, A., Tadi, B.Y. and Golestanian, H. (2019), "Size Dependent Nonlinear Bending Analysis of a Flexoelectric Functionally Graded Nano-Plate Under Thermo-Electro-Mechanical Loads", *J. Solid. Mech.*, **12**(1), 33-56. https://doi.org/10.22034/JSM.2019.569280.1296.

Guo, Y. and Jinghui, Z. (2004), "Shock Absorbing Characteristics and Vibration Transmissibility of Honeycomb Paperboard", *Shock Vib.*, **11**(5,6), 521-531.

He, L., Lou, J., Zhang, E., Wang, Y. and Bai, Y. (2015), "A size-dependent four variable refined plate model for functionally graded microplates based on modified couple stress theory", *Compos. Struct.*, **130**, 107-115. https://doi.org/10.1016/j.compstruct.2015.04.033.

Hebali, H., Tounsi, A., Sid, M. and Bessaim, A. (2014), "New Quasi-3D hyperbolic shear deformation theory for the static and free vibration analysis of functionally graded plates", *J. Eng. Mech.*, **140**, 374-383. https://doi.org/10.1061/(ASCE)EM.1943-7889.0000665.

Hirwani, C.K. and Panda, S.K. (2019a), "Nonlinear thermal free vibration frequency analysis of delaminated shell panel using FEM", *Compos. Struct.*, **224**, 111011. https://doi.org/10.1016/j.compstruct.2019.111011.

Hirwani, C.K. and Panda, S.K. (2018), "Numerical nonlinear frequency analysis of pre-damaged curved layered composite structure using higher-order finite element method", *Int. J. Nonlinear Mech.*, **102**, 14-24. https://doi.org/10.1016/j.ijnonlinmec.2018.03.005.

Hirwani, C.K. and Panda, S.K. (2019b), "Nonlinear finite element solutions of thermoelastic deflection and stress responses of internally damaged curved panel structure", *Appl. Math. Model.*, **65**, 303-317. https://doi.org/10.1016/j.apm.2018.08.014.

Hu, S., Shen, S., Shuling, H.U. and Shengping, S. (2010), "Variational principles and governing equations in nano-dielectrics with the flexoelectric effect", *Sci. China Phys. Mech. Astronomy*, **53**(8), 1497-1504. https://doi.org/10.1007/s11433-010-4039-5.

Jafari Mehrabadi, S., Sobhani Aragh, B., Khoshkhahesh, V. and Taherpour, A. (2012), "Mechanical buckling of nanocomposite rectangular plate reinforced by aligned and straight single-walled carbon nanotubes", *Compos. Part B: Eng.*, **43**(4), 2031-2040. https://doi.org/10.1016/j.compositesb.2012.01.067.

Katariya, P.V. and Panda, S.K. (2019a), "Frequency and deflection responses of shear deformable skew sandwich curved shell panel: A finite element approach", *Arab. J. Sci. Eng.*, **44**(2), 1631-1648. https://doi.org/10.1007/s13369-018-3633-0.

Katariya, P.V., Panda, S.K. and Mahapatra, T.R. (2018), "Bending and vibration analysis of skew sandwich plate", *Aircr. Eng. Aerosp. Tech.*, **90**(6), 885-895. https://doi.org/10.1108/AEAT-05-2016-0087.

Katariya, P.V. and Panda, S.K. (2019b), "Numerical frequency analysis of skew sandwich layered composite shell structures under thermal environment including shear deformation effects", *Struct. Eng. Mech., Int. J.*, **71**(6), 657-668. https://doi.org/10.12989/sem.2019.71.6.657

Khorasani, M., Eyvazian, A., Karbon, M., Tounsi, A., Lampani, L., Sebaey, T.A. and Sebaey, T.A. (2020), "Magneto-electro-elastic vibration analysis of modified couple stress-based three-layered micro rectangular plates exposed to multi-physical fields considering the flexoelectricity effects", *Smart Struct. Syst., Int. J.*, **26**(3), 331-343. https://doi.org/10.12989/SSS.2020.26.3.331.

Khorasani, M., Soleimani-Javid, Z., Arshid, E., Lampani, L. and Civalek, Ö. (2021), "Thermo-elastic buckling of honeycomb micro plates integrated with FG-GNPs reinforced Epoxy skins with stretching effect", *Compos. Struct.*, **258**, 113430. https://doi.org/10.1016/j.compstruct.2020.113430.

Kumar, S. and Renji, K. (2019), "Estimation of strains in composite honeycomb sandwich panels subjected to low frequency diffused acoustic field", *J. Sound. Vib.*, **449**, 84-97. https://doi.org/10.1016/j.jsv.2019.02.013.

Li, Y. and Jin, Z. (2008), "Free flexural vibration analysis of symmetric rectangular honeycomb panels with SCSC edge supports", *Compos. Struct.*, **83**(2), 154-158. https://doi.org/10.1016/j.compstruct.2007.04.004.

Liu, C., Hu, S. and Shen, S. (2012), "Effect of flexoelectricity on electrostatic potential in a bent piezoelectric nanowire", *Smart Mater. Struct.*, **21**(11), 115024. https://doi.org/10.1088/0964-1726/21/11/115024.

Liu, J., Cheng Y.S. and Lirf, A.U. (2010), "A semi-analyrical method for bending, buckling, and free vibration analyses of sandwich panels with square-honeycomb cores", *Int. J. Struct. Stab. Dyn.*, **10**(01), 127-151. https://doi.org/10.1142/S0219455410003361.

Ma, W. and Cross, L.E. (2001), "Observation of the flexoelectric effect in relaxor $Pb(Mg_{1/3}Nb_{2/3})O_3$ ceramics", *Appl. Phys. Lett.*, **78**(19), 2920-2921. https://doi.org/10.1063/1.1356444.

Ma, W. and Cross, L.E. (2002), "Flexoelectric polarization of barium strontium titanate in the paraelectric state", *Appl. Phys. Lett.*, **81**(18), 3440-3442. https://doi.org/10.1063/1.1518559.

Ma, W. and Cross, L.E. (2006), "Flexoelectricity of barium titanate", *Appl. Phys. Lett.*, **88**(23), 2004-2007. https://doi.org/10.1063/1.2211309.

Maheri, M.R. and Adams, R.D. (1994), "Steady-state flexural vibration damping of honeycomb sandwich beams", *Compos. Sci. Technol.*, **52**(3), 333-347. https://doi.org/10.1016/0266-3538(94)90168-6.

Maranganti, R., Sharma, N.D. and Sharma, P. (2006), "Electromechanical coupling in nonpiezoelectric materials due to nanoscale nonlocal size effects: Green's function solutions and embedded inclusions", *Phys. Rev. B.*, **74**(1), 1-14. https://doi.org/10.1103/PhysRevB.74.014110.

Mashkevich, V.S. (1957), "Electrical, Optical, and Elastic Properties of Diamond-Type Crystals", *J. Exptl. Theoret. Phys.*, **5**(4), 707-713.

Mehar, K., Mishra, P.K. and Panda, S.K. (2020a), "Numerical investigation of thermal frequency responses of graded hybrid smart nanocomposite (CNT-SMA-Epoxy) structure", *Mech. Adv. Mater. Struct.*, 1-13. https://doi.org/10.1080/15376494.2020.1725193.

Mehar, K., Mahapatra, T.R., Panda, S.K., Katariya, P.V. and Tompe, U.K. (2018), "Finite-element solution to nonlocal elasticity and scale effect on frequency behavior of shear deformable nanoplate structure", *J. Eng. Mech.*, **144**(9), 04018094. https://doi.org/10.1061/(ASCE)EM.1943-7889.0001519.

Mehar, K., Panda, S.K. and Sharma, N. (2020b), "Numerical investigation and experimental verification of thermal frequency of carbon nanotube-reinforced sandwich structure", *Eng. Struct.*, **211**, 110444. https://doi.org/10.1016/j.engstruct.2020.110444.

Mehrabadi, S.J., Aragh, B.S., Khoshkhahesh, V. and Taherpour, A. (2012), "Mechanical buckling of nanocomposite rectangular plate reinforced by aligned and straight single-walled car", *Compos. Part B-Eng.*, **43**(4), 2031-2040. https://doi.org/10.1016/j.compositesb.2012.01.067

Mindlin, R.D. (1968), "Polarization gradient in elastic dielectrics", *Int. J. Solids. Struct.*, **4**(6), 637-642. https://doi.org/10.1016/0020-7683(68)90079-6.

Mukhopadhyay, T. and Adhikari, S. (2016), "Free-Vibration analysis of sandwich panels with randomly irregular Honeycomb Core", *J. Eng. Mech.*, **142**, 06016008. https://doi.org/10.1061/(ASCE)EM.1943-7889.0001153.

Nakamoto, H., Adachi, T. and Araki, W. (2009), "In-plane impact behavior of honeycomb structures filled with linearly arranged inclusions", *Int. J. Impact Eng.*, **36**(8), 1019-1026. https://doi.org/10.1016/j.ijimpeng.2009.01.004.

Nguyen, T.D., Mao, S., Yeh, Y.-W., Purohit, P.K. and McAlpine, M.C. (2013), "Nanoscale Flexoelectricity", *Adv. Mater.*, **25**(7), 946-974. https://doi.org/10.1002/adma.201203852.

Patle, B.K., Hirwani, C.K., Singh, R.P. and Panda, S.K. (2018), "Eigenfrequency and deflection analysis of layered structure using uncertain elastic properties - a fuzzy finite element approach", *Int. J. Approx. Reason.*, **98**, 163-176. https://doi.org/10.1016/j.ijar.2018.04.013.

Sahoo, S.S., Panda, S.K., Mahapatra, T.R. and Hirwani, C.K. (2019), "Numerical Analysis of Transient Responses of Delaminated Layered Structure Using Different Mid-plane Theories and Experimental Validation", *Irann. J. Sci. Technol.*, **43**(1), 41-56. https://doi.org/10.1007/s40997-017-0111-3.

Salari, E., Ashoori, A. and Vanini, S.A.S. (2019), "Porosity-dependent asymmetric thermal buckling of inhomogeneous annular nanoplates resting on elastic substrate", *Adv. Nano. Res., Int. J.*, **7**(1), 25-38. https://doi.org/10.12989/anr.2019.7.1.025.

Shariati, A., Ebrahimi, F., Karimiasl, M., Vinyas, M. and Toghroli, A. (2020), "On transient hygrothermal vibration of embedded viscoelastic flexoelectric/piezoelectric nanobeams under magnetic loading", *Adv. Nano. Res., Int. J.*, **8**(1), 49-58. https://doi.org/10.12989/anr.2020.8.1.049.

Sharma, N.D., Landis, C.M. and Sharma, P. (2010), "Piezoelectric thin-film super-lattices without using piezoelectric materials", *J. Appl. Phys.*, **108**(2), 024304. https://doi.org/10.1063/1.3443404.

Sharma, N.D.D., Maranganti, R. and Sharma, P. (2007), "On the possibility of piezoelectric nanocomposites without using piezoelectric materials", *J. Mech. Phys. Solids*, **55**(11), 2328-2350. https://doi.org/10.1016/j.jmps.2007.03.016.

Shen, S. and Hu, S. (2010), "A theory of flexoelectricity with surface effect for elastic dielectrics", *J. Mech. Phys. Solids*, **58**(5), 665-677. https://doi.org/10.1016/j.jmps.2010.03.001.

Shingare, K.B. and Kundalwal, S.I. (2020), "Flexoelectric and surface effects on the electromechanical behavior of graphene-based nanobeams", *Appl. Math. Model.*, **81**, 70-91. https://doi.org/10.1016/j.apm.2019.12.021.

Shu, L., Wei, X., Pang, T., Yao, X. and Wang, C. (2011), "Symmetry of flexoelectric coefficients in crystalline medium", *J. Appl. Phys.*, **110**(10), 104106. https://doi.org/10.1063/1.3662196.

Singh, V.K., Hirwani, C.K., Panda, S.K., Mahapatra, T.R. and Mehar, K. (2019), "Numerical and experimental nonlinear dynamic response reduction of smart composite curved structure using collocation and non-collocation configuration", *Proceedings of the Institution of Mechanical Engineers, Part C: Journal of Mechanical Engineering Science*, **233**(5), 1601-1619. https://doi.org/10.1177/0954406218774362.

Singh, V.K., Mahapatra, T.R. and Panda, S.K. (2016a), "Nonlinear flexural analysis of single/doubly curved smart composite shell panels integrated with PFRC actuator", *Eur. J. Mech. A-Solid.*, **60**, 300-314. https://doi.org/10.1016/j.euromechsol.2016.08.006.

Singh, V.K., Mahapatra, T.R. and Panda, S.K. (2016b), "Nonlinear transient analysis of smart laminated composite plate integrated with PVDF sensor and AFC actuator", *Compos. Struct.*, **157**, 121-130. https://doi.org/10.1016/j.compstruct.2016.08.020.

Singh, V.K. and Panda, S.K. (2015), "Large amplitude free vibration analysis of laminated composite spherical shells embedded with piezoelectric layers", *Smart Struct. Syst., Int. J.*, **16**(5), 853-872. http://doi.org/10.12989/sss.2015.16.5.853.

Sobhy, M. (2020), "Differential quadrature method for magneto-hygrothermal bending of functionally graded graphene/Al sandwich-curved beams with honeycomb core via a new higher-order theory", *J. Sandw. Struct. Mater.*, 1099636219900668. https://doi.org/10.1177/1099636219900668.

Tagantsev, A.K. (1986), "Piezoelectricity and flexoelectricity in crystalline dielectrics", *Phys. Rev. B*, **34**(8), 5883-5889. https://doi.org/10.1103/PhysRevB.34.5883.

Tagantsev, A.K. and Gerra, G. (2006), "Interface-induced phenomena in polarization response of ferroelectric thin films", *J. Appl. Phys.*, **100**(5), 051607. https://doi.org/10.1063/1.2337009.

Thai, H.T. and Choi, D.H. (2013), "Size-dependent functionally graded Kirchhoff and Mindlin plate models based on a modified couple stress theory", *Compos. Struct.*, **95**, 142-153. https://doi.org/10.1016/j.compstruct.2012.08.023.

Yang, W., Liang, X. and Shen, S. (2015), "Electromechanical responses of piezoelectric nanoplates with flexoelectricity", *Acta Mechanica*, **226**(9), 3097-3110. https://doi.org/10.1007/s00707-015-1373-8.

Yudin, P.V. and Tagantsev, A.K. (2013), "Fundamentals of flexoelectricity in solids", *Nanotechnology*, **24**(43), 432001. https://doi.org/10.1088/0957-4484/24/43/432001.

Zeng, S., Wang, B.L. and Wang, K.F. (2019), "Nonlinear vibration of piezoelectric sandwich nanoplates with functionally graded porous core with consideration of flexoelectric effect", *Compos. Struct.*, **207**, 340-351. https://doi.org/10.1016/j.compstruct.2018.09.040.

Zenkour, A.M. (2016), "Buckling of a single-layered graphene sheet embedded in visco-Pasternak", *Adv. Nano. Res., Int. J.*, **4**(4), 309-326. https://doi.org/10.12989/anr.2016.4.4.309.

Zhang, Z. and Jiang, L. (2014), "Size effects on electromechanical coupling fields of a bending piezoelectric nanoplate due to surface effects and flexoelectricity", *J. Appl. Phys.*, **116**, 134308. https://doi.org/10.1063/1.4897367.

Zhang, Z., Yan, Z. and Jiang, L. (2014), "Flexoelectric effect on the electroelastic responses and vibrational behaviors of a piezoelectric nanoplate", *J. Appl. Phys.*, **116**(1), 014307. https://doi.org/10.1063/1.4886315.

Zhao, M., Qian, C., Lee, S.W.R., Tong, P., Suemasu, H. and Zhang, T.-Y. (2007), "Electro-elastic analysis of piezoelectric

laminated plates", *Adv. Compos. Mater.*, **16**(1), 63-81. https://doi.org/10.1163/156855107779755273.

Zubko, P., Catalan, G. and Tagantsev, A.K. (2013), "Flexoelectric Effect in Solids", *Annual Rev. Mater. Res.*, **43**(1), 387-421. https://doi.org/10.1146/annurev-matsci-071312-121634.

CC